Modeling and Measuring Eccentricity in Binary Black Hole Inspirals

Interim Report 2, LIGO Student Undergraduate Research Fellowship, California Institute of Technology

Simona Miller

Smith College, Northampton, MA 01063

Mentors: Alan Weinstein and Jonah B. Kanner

LIGO Laboratory, Caltech, Pasadena, CA 91125

(Dated: August 3, 2018)

Abstract

Due to the emission of gravitational wave (GW) radiation, most compact binaries are expected to circularize before emitting GW in the LIGO frequency band. However, if a binary black hole system resulted from dynamical capture or hierarchal triple interactions close to the end of its life, there is a probability that the system could retain non-negligible eccentricity while in the LIGO band. As such, observing eccentricity from a gravitational wave signal could be a clear signature of dynamical origins. Despite the observational importance of eccentricity, the techniques needed to detect and characterize it currently remain in their early stages. We seek to model and assess detectability and identifiability of eccentric binary black hole systems, aiming to discover how accurately we can estimate parameters of an eccentric waveform. In particular, we search for degeneracies between eccentricity and other higher order effects, such as spin precession. We employ a variety of data analysis techniques, including calculating overlaps between waveforms, constructing likelihood distributions, and performing Bayesian inference.

I. INTRODUCTION

To date, LIGO's gravitational wave detectors have observed gravitational waves from six binary black holes and one binary neutron star [1–6]. The observed binary black hole (BBH) coalescences follow a consistent pattern: the systems have quasi-circular orbits that decrease in radius and increase in frequency as they lose energy in the form of gravitational radiation. All observed gravitational waves from BBH fit a "chirp" waveform while within the LIGO frequency band (a minimal orbital frequency of 10 Hz, or a gravitational wave frequency of 20 Hz); their amplitude and frequency increase as the binary evolves [19]. The plots in Figure 1 show predicted chirp waveforms; Figure 2 shows an "actual" waveform, or bandpassed, filtered data from GW150914, LIGO's first detected gravitational wave [12]. Although General Relativity predicts subtle effects from eccentricity, LIGO data analysis methodology presently uses waveform templates that assume a negligible eccentricity; highly eccentric BBH could go undetected with current technology. Additionally, many properties of BBH are currently calculated with the assumption of circular orbits, such as their distance from Earth [19]. Identifying eccentricity could make such calculations more accurate, and will yield a better understanding BBH formation mechanisms and the stellar environments in which they reside.

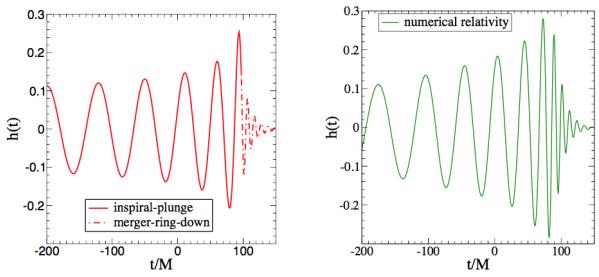

FIG. 1: Chirp waveform predicted using effective-one-body approach (left) and numerical relativity simulations (right) for same initial conditions. Figure from [19]

In this report, I describe the work with the "eccentricity problem" that I have thus completed this summer. Section II outlines the objectives for this project. In Section III, I describe binary black hole formation mechanisms that could result in measurable eccentricity. In Section IV, I discuss how orbital period, semi-major major axis, and eccentricity evolve over time during an eccentric inspiral. Section V introduces waveforms for BBH with eccentricity; here I present the equations for the emitted gravitational wave strain and

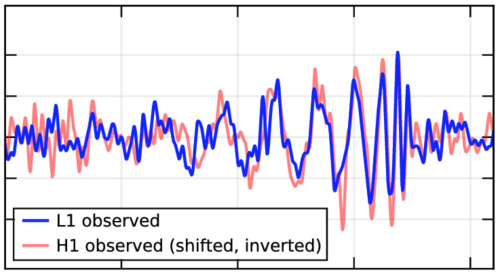

FIG. 2: Strain (h(t)) plotted against time (t) for GW150914, LIGO's first GW detection. This plot shows data that has been filtered, i.e. subject to band-passing and line removal. L1 is the data from the Livingston, Louisiana detector; H1 is the data from the Hanford, Washington detector. Figure from [12]

describe unique characteristics of such waveforms. In Section VI, I describe the Bayesian Inference framework used for data analysis. In Section VII, I present interim results. Challenges that I have thus encountered are discussed in Section VIII, and an outline for the remainder of the summer is given in Section IX.

II. OBJECTIVES

The aim of this project is to build on existing research to assess detectability and identifiability of eccentric binary black holes. We will focus on three groups of questions:

1. What are key features of eccentric waveforms in the time and frequency domains? In Python, we will create a waveform family for a range of initial eccentricities using a lowest order Parametrized Post-Newtonian approximation and compare these waveforms to existing models in LALSuite. As a function of phase difference, how do these eccentric waveforms deviate from quasi-circular waveforms?

2. Does eccentricity make GW signals from BBH harder to detect? Specifically, how much signal-to-noise ratio (SNR) can be lost if a search pipeline use a quasi-circular binary template (with no higher order effects) to capture an eccentric binary merger event? We will calculate this as a function of the initial eccentricity (e.g. eccentricity at GW frequency of 20 Hz) and the masses of the two black holes.

3. How well can the eccentricity parameter be extracted from an observed event, using Bayesian parameter estimation and MCMC techniques? Are there any degeneracies

between eccentricity and chirp mass, mass ratio, and/or spin that affect our ability to extract the eccentricity parameter from a data set? Furthermore, are there any degeneracies between eccentricity and other higher order effects like spin precession?

III. BINARY BLACK HOLE FORMATION MECHANISMS

Binary black holes have several formation mechanisms, the two most widely understood being common binary evolution and dynamical interaction in dense stellar environments such as globular clusters or galactic nuclei. Evolutionary trajectories for both formation mechanisms predict that under most circumstances, the orbits of BBH systems will have circularized by the time their emitted gravitational radiation is within the LIGO band. However, if a BBH forms via dynamical capture with an extremely large eccentricity and/or extremely close to the end of its lifetime (i.e., a small periastron), there *is* a probability that the system could be detected using quasi-circular templates while still in a non-circular orbit [1]. Dense stellar regions, such as galactic nuclei and globular clusters that have undergone mass segregation, are prime spots for dynamical BH-BH capture. In such settings, individual black holes can become gravitationally bound during close passage as energy is lost in the form of a GW burst[10].

Another possibility for observing an eccentric BBH in the LIGO band is via a hierarchal triple, a quasi-stable three-body system where one BBH is orbited by another black hole. Ellipticity can be produced in hierarchal triples through angular momentum exchange from the inner binary and the larger system, in what is known as the Kozai-Lidov mechanism [13, 17].

IV. ECCENTRIC BINARY INSPIRAL EVOLUTION

The evolution of compact binary coalescences can be broken into three phases: inspiral, merger, and ringdown. We focus on the inspiral phase, as once the CBC enters merger eccentricity no longer produces distinguishable effects. The inspiral phase is the longest phase in a CBC, ending when the objects reach their innermost stable circular orbit (ISCO). This occurs at the following condition for semi-major axis length a:

$$a_{ISCO} = 6\ \frac{G\,(\,m_1\,+\,m_2\,)}{c^2} \quad . \tag{1}$$

In his paper "Gravitational Radiation from Post-Newtonian Sources and Inspiralling Compact Binaries," Luc Blanchet derives the following coupled lowest order ordinary differential equations describing period decay and eccentricity decay of a BBH during the inspiral phase [7]:

$$\dot{P}_{orb} = -\frac{192\pi}{5c^5}\left(\frac{2\pi G}{P_{orb}}\right)^{5/3}\frac{m_1 m_2}{(m_1+m_2)^{1/3}}\left(1+\frac{73}{24}e^2+\frac{37}{96}e^4\right)\left(1-e^2\right)^{-7/2} \quad , \tag{2}$$

$$\dot{e} = -\frac{608\pi}{15c^5}\frac{e}{P_{orb}}\frac{m_1 m_2}{(m_1+m_2)^{1/3}}\left(1+\frac{121}{304}e^2\right)\left(1-e^2\right)^{-5/2} \quad . \tag{3}$$

It is important to note that these equations ignore spin effects and higher order effects, such as spin precession or higher order modes. Blanchet integrates analytically to determine that orbital period and eccentricity are related via

$$c_0 P^{19/9} = \frac{e^2}{(1-e^2)^{19/6}}\left(1+\frac{121}{304}e^2\right)^{145/121} \tag{4}$$

where c_0 is a constant determined by the initial conditions of the orbit. Numerically solving (2) and (3) with the initial conditions of $P_{orb,0} = 0.3s$ and $e_0 = 0.4$ yields the time series for orbital period and eccentricity shown in Figure 3. Additionally, a time series for semi-major axis length a was calculated from Kepler's Third Law (also seen in Figure 3),

$$a = \left[{P_{orb}}^2\left(\frac{G(m_1+m_2)}{4\pi^2}\right)\right]^{1/3} \quad . \tag{5}$$

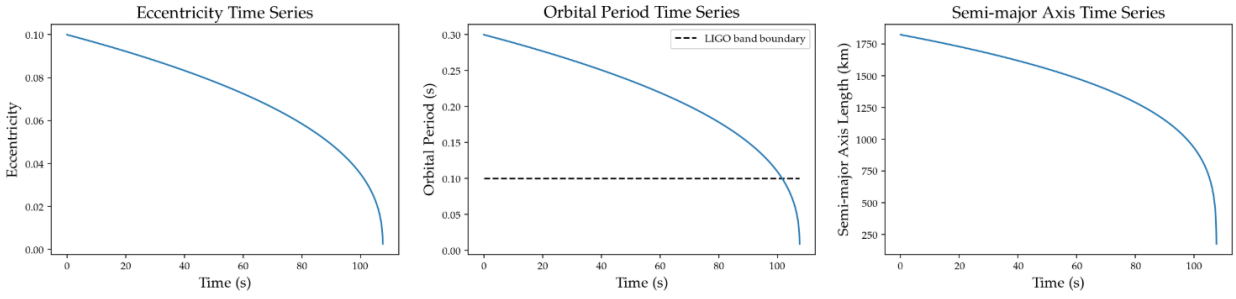

FIG. 3: Time evolution of eccentricity, orbital period, and semi-major axis for BBH system with initial orbital period of 0.3 seconds and initial eccentricity of 0.1.

The shape of the time series' for orbital period and eccentricity depend on initial orbital period, initial eccentricity, chirp mass, and mass ratio. As initial eccentricity, or for our purposes, the eccentricity at an orbital period of 0.1s (corresponding to the lowest frequency in the LIGO band) increases, the duration of the CBC in the LIGO band decreases; the BBH reaches ISCO in a shorter amount of time. As total mass increases and/or mass ratio decreases, the duration of the BBH in the LIGO band also decreases. These patterns can be seen in Figures 4, 5, and 6.

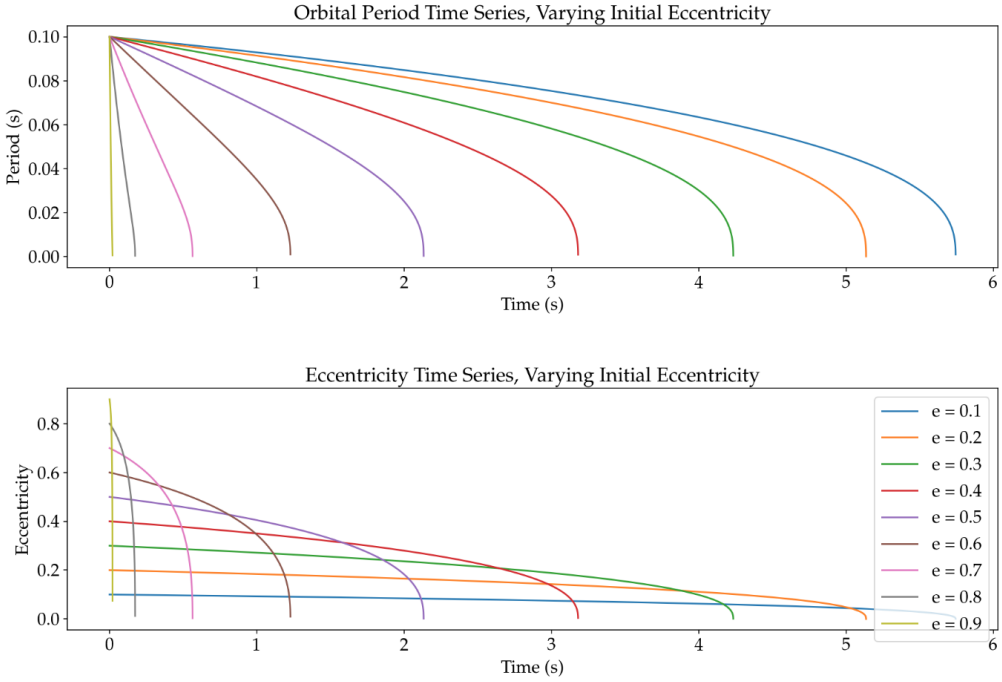

FIG. 4: Orbital period time series and eccentricity time series with varying values of eccentricity at an initial period of 0.1s.

V. WAVEFORM MODELS

Once a dynamically captured BH pair is in eccentric orbit, a GW burst is theorized to be emitted every time the pair passes at a close encounter (i.e. at periastron). This causes the semi-major axis (a) and eccentricity (e) to decrease with time, while orbital frequency increases with time. After sufficient energy is lost through gravitational radiation, the BH pair will merge.

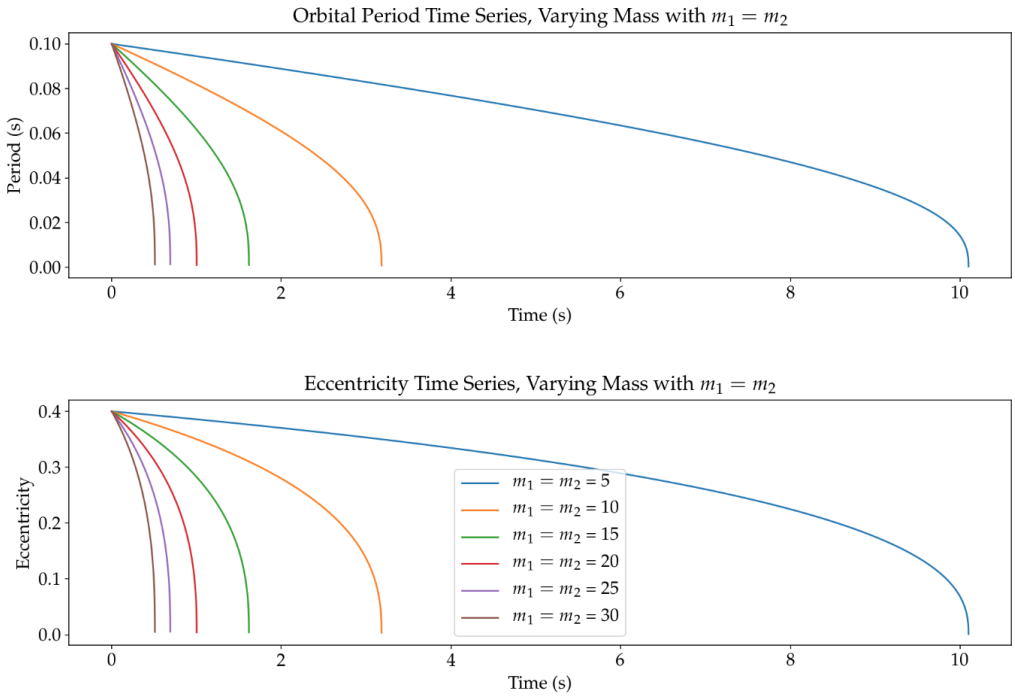

FIG. 5: Orbital period time series and eccentricity time series with varying total masses. All series have a mass ratio of 1.

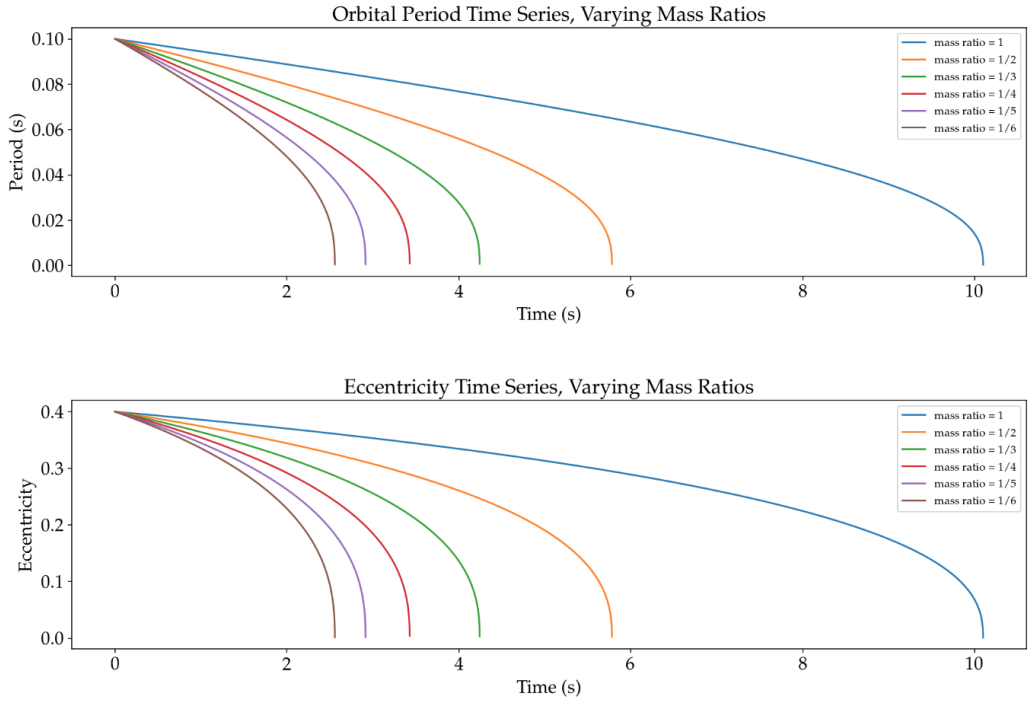

FIG. 6: Orbital period time series and eccentricity time series with varying mass ratios. m_1 always equals 5 solar masses, and m_2 ranges from 5 solar masses to 35 solar masses in increments of 5 solar masses.

A. Generating a Waveform Model using Python

Gravitational wave strain, $h(t)$ is generated by an accelerating quadrupole moment, I: $h(t) \sim \frac{d^2}{dt^2}(I)$ where $I = \int \rho\, r^2\, dV$. Without taking the effects of eccentricity into account, this strain is optimized in (6) where d is the distance to the source, a is the distance between the orbiting bodies, m_1 and m_2 are the masses of the BH, and $\varphi(t)$ is the phase evolution:

$$h(t) = \left(\frac{2G(m_1 + m_2)}{c^2 d}\right)\left(\frac{2G(m_1 + m_2)}{c^2 a}\right) cos(2\,\varphi(t)) \quad . \tag{6}$$

However, BBH in eccentric orbits produce a more complicated GW strain, due to emitting GW bursts at periastron passage, periastron precession, and the consequent oscillating distance between the orbiting bodies. The location of a body in an eccentric orbit can be defined using two angles: ψ and ϕ. ψ, also know as the true anomaly, corresponds to the radial period; it is taken with respect to the semi-major axis. However, due to periastron precession, the semi-major axis is itself rotating. ϕ takes this into account; it corresponds to the orbital period. It is taken from a fixed axis in space, while the axis from which ψ is taken is rotating. See Figure 7 for a visualization.

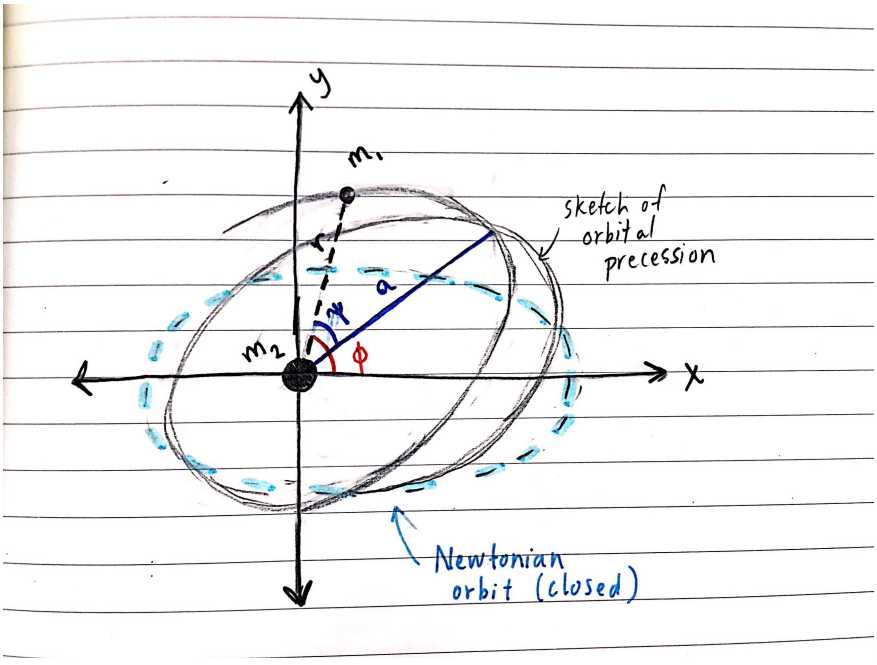

FIG. 7: Diagram showing difference between ϕ and ψ in an eccentric binary. ϕ is the angle between r and a fixed x-axis in m_2's (the larger mass) frame of reference, while ψ is the angle between r and the precessing semi-major axis a.

Taking these effects into account, the plus and cross polarizations for gravitational wave strain from an eccentric BBH system are:

$$h_+(t) = \frac{\mu}{2\,D}\Bigg(\Big[1\,-\,2\,cos\big(2\theta\big)\,cos^{\,2}\big(\phi(t)\big) - 3\,cos\big(2\,\phi(t)\big)\Big]\dot{r}^{\,2}(t) + \Big(3\,+\,cos\big(2\theta\big)\Big)\Big[2\,cos\big(2\,\phi(t)\big)\,\dot{\phi}^{\,2}(t) + \,sin\big(2\,\phi(t)\big)\,\ddot{\phi}(t)\Big]r^{\,2}(t) + \Big[4\Big(3\,+\,cos\big(2\theta\big)\Big)\,sin\big(2\,\phi(t)\big)\dot{\phi}(t)\dot{r}(t) + \Big(1\,-\,2\,cos\big(2\theta\big)\,cos^{\,2}\big(\phi(t)\big)\,-\,3\,cos\big(2\phi(t)\big)\Big)\ddot{r}(t)\Big]r(t)\Bigg) \quad , \quad (7)$$

$$h_\times(t) = -\frac{2\,\mu\,cos(\theta)}{D}\Bigg(sin\big(2\phi(t)\big)\,\dot{r}^2(t) + \Big[cos\big(2\phi(t)\big)\,\ddot{\phi}(t)\,-\,2\,sin\big(2\phi(t)\big)\,\dot{\phi}^2(t)\Big]r^2(t) + \Big[4\,cos\big(2\phi(t)\big)\,\dot{\phi}(t)\,\dot{r}(t)\,+\,sin\big(2\phi(t)\big)\,\ddot{r}(t)\Big]r(t)\Bigg) \quad (8)$$

where μ is the reduced mass of the binary, D is the distance to the source, θ is the angle of inclination of the source, r is the distance between the two BHs, and ϕ is angle corresponding to the orbital period [9].

To solve for the strain, we need to time evolve r and ϕ, which is done using the energy and angular momentum of the system. In this derivation we use the Newtonian approximations of these quantities. The Newtonian definition of orbital energy E_{orb} for an elliptical orbit with total mass M_{tot}, reduced mass μ, and semi-major axis length a is, in Joules:

$$E_{orb} = K + U = \frac{U}{2} = -\frac{G\,M_{tot}\,\mu}{2a} \quad (9)$$

where $K + U = \frac{U}{2}$ is the Virial Theorem for gravity. The Newtonian definition of orbital angular momentum L_{orb} is as follows, in $kg\,m^2/s$:

$$L_{orb} = \sqrt{G\,M_{tot}\,\mu\,a\,(1\,-\,e^2)} \quad . \quad (10)$$

From these definitions, we can express the quantities of specific total energy and specific

angular momentum, in geometric units (G=c=1), to be used throughout the remainder of the report:

$$E = 1 + \frac{E_{orb}}{\mu} \quad , \quad L = \frac{L_{orb}}{\mu} \quad . \tag{11}$$

The distance r between the two BH's is:

$$r = \frac{a\left(1 - e^2\right)}{1 + e\, cos\psi} \tag{12}$$

where ψ is the true anomaly of the eccentric system (see Figure 7). To generate a time series for r, we must time evolve ψ using the following equation, adapted from [9]:

$$\dot{\psi} = \frac{(1\ -\ E^2)^{1/2}}{V_t\,(1\ -\ e^2)} \Big[a\,(1 - e^2)\ - C_0\,(1 - e)\ -\ e\,a\,(1 - e^2) - e\,C_0\,(1 - e)\,cos(\psi)\Big]^{1/2} \Big[a\,(1 - e^2)\,(1 + e)\Big]^{1/2} \tag{13}$$

where the constant C_0 is given by:

$$C_0 = \frac{2}{1 - E^2} - 2a \tag{14}$$

and potential V_t is given by:

$$V_t = \frac{E\, r^4}{r^2\ -\ 2r} \tag{15}$$

.

Finally, to solve the gravitational wave strain equations given in (7) and (8), we must generate a time series for ϕ, the angle describing where a body is in its orbital period (see Figure 7). This is achieved with the following relationship between $\dot{\phi}$, specific angular momentum, and potential V_t [9]:

$$\dot{\phi} = \frac{L}{V_t} \quad . \tag{16}$$

Choosing an initial period and eccentricity, solving for the time evolution of r and ϕ, and substituting into (7) and (8) yields the time series shown in Figure 8. This model shows the

unique feature appearing in a waveform generated by a BBH system in an eccentric orbit: bursts of gravitational wave radiation produced at periastron passage. As initial eccentricity increases, these bursts increases in magnitude. Additionally, just like non-eccentric waveforms, this model shows the characteristic chirp behavior of a CBC: amplitude and frequency of the the GW strain increase as the binary evolves.

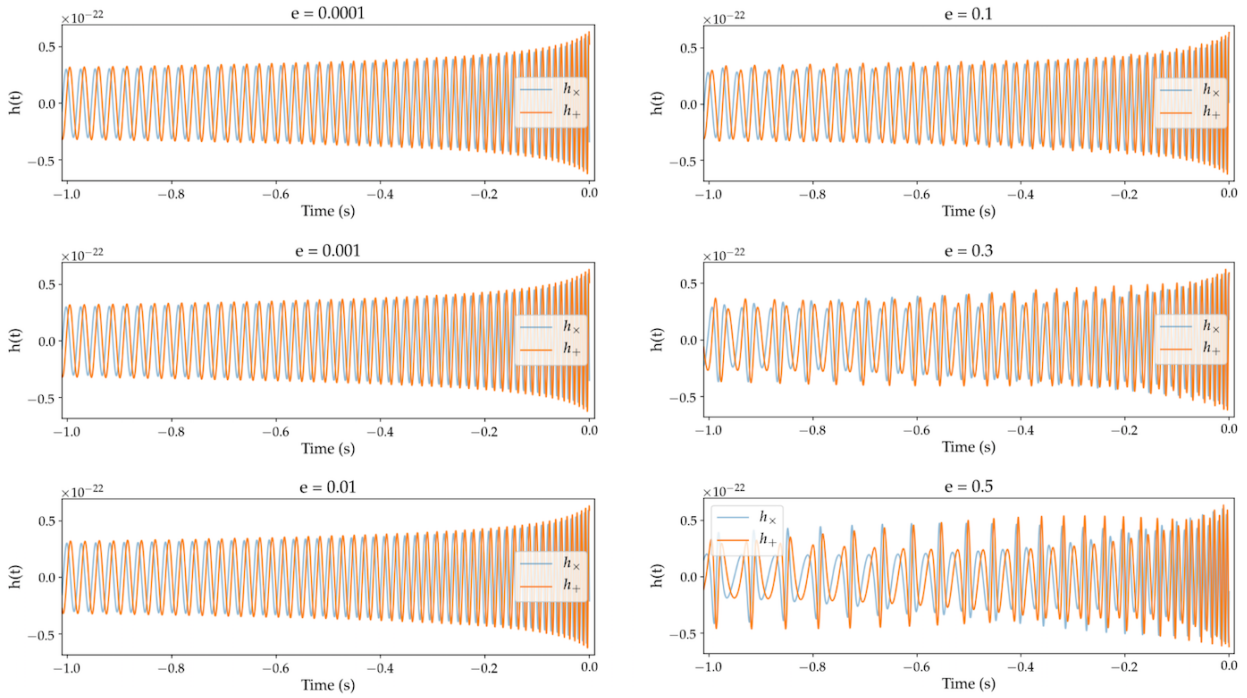

FIG. 8: Time series waveforms generated by the model described in Section V A. with initial orbital period $P_0 = 0.1s$ and initial eccentricities e_0=[0.0001, 0.001, 0.01, 0.1, 0.3, 0.5]. All waveforms are from a source with a distance of 1000 megaparsecs, masses $m_1 = m_2 = 10M_\odot$, and an inclination angle $\theta = \pi/4$. All plots show the final second before merger.

Although the model I created captures the key qualitative features of an eccentric BBH inspiral, the Newtonian approximations made for energy and angular momentum prevent it from being quantitatively accurate. Future work for this project might include improving this waveform model. Because of this inaccuracy, the EccentricTD and EccentricFD models (see Section V B.) are used for data analysis in the remainder of this report. See Section VII A for quantitative measurements of this discrepancy.

B. Existing Models

Presently, only one waveform model in the time domain - EccentricTD - and one model in the frequency domain - EccentricFD - that include the effects of eccentricity exist in the LIGO Scientific Collaboration Algorithm Library Suite (LALSuite) [11]. Like the waveforms generated in Section V A, these waveform families only model the inspiral phase of a CBC. Examples of time series plotted with EccentricTD and frequency series plotted with EccentricFD with varying initial eccentricity values can be seen in Figures 9 and 10. Note that the right three plots in Figure 10 are noisy. At this time we are unsure if this effect is due to physical reasons, inherent problems with the EccentricFD waveform, under-sampling in the frequency domain, or some other cause.

Models including the merger and ringdown phases of an eccentric CBC *have* been calculated, such as in the paper "Observing complete gravitational wave signals from dynamical capture binaries" by East et al [10]; these models have not yet been incorporated into LALSuite. See Figure 11 for a plot of an example of a full inspiral-merger-ringdown time series.

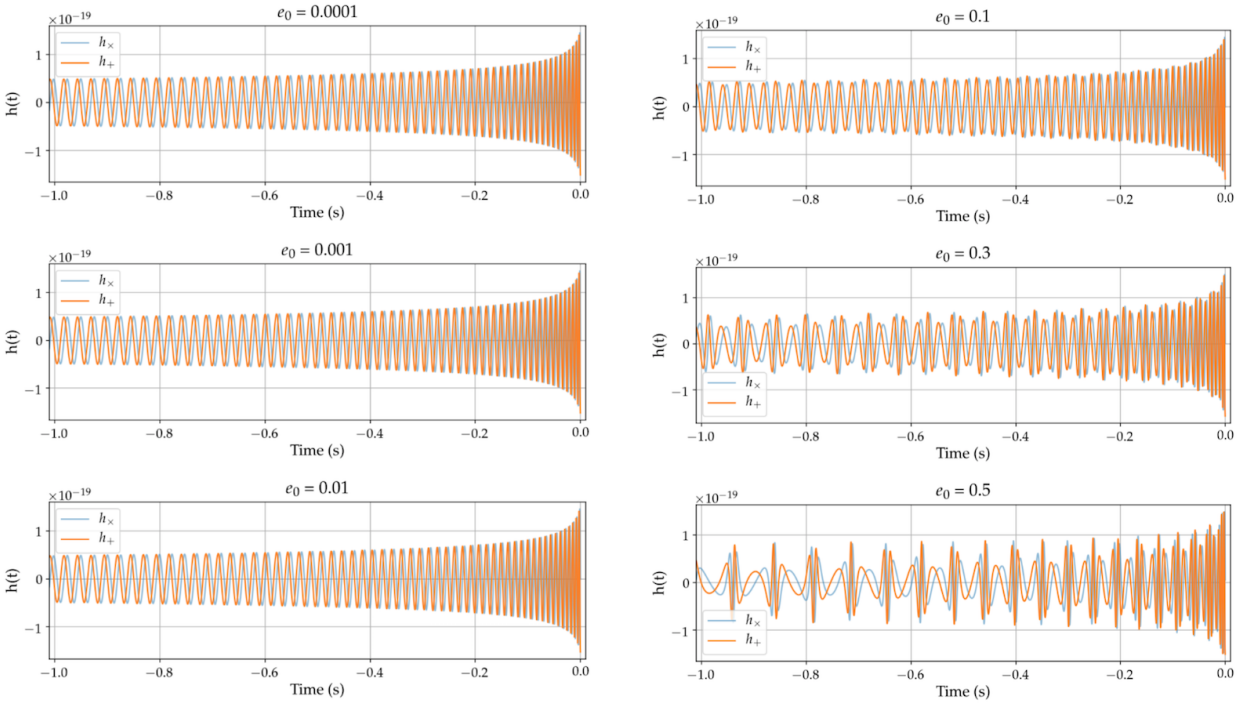

FIG. 9: Time series waveforms generated with the EccentricTD approximant at initial eccentricities e_0=[0.0001, 0.001, 0.01, 0.1, 0.3, 0.5]. All waveforms are from a source with a distance of 1 megaparsec and masses $m_1 = m_2 = 10M_\odot$. All plots show the final second before merger. Approximant from [11].

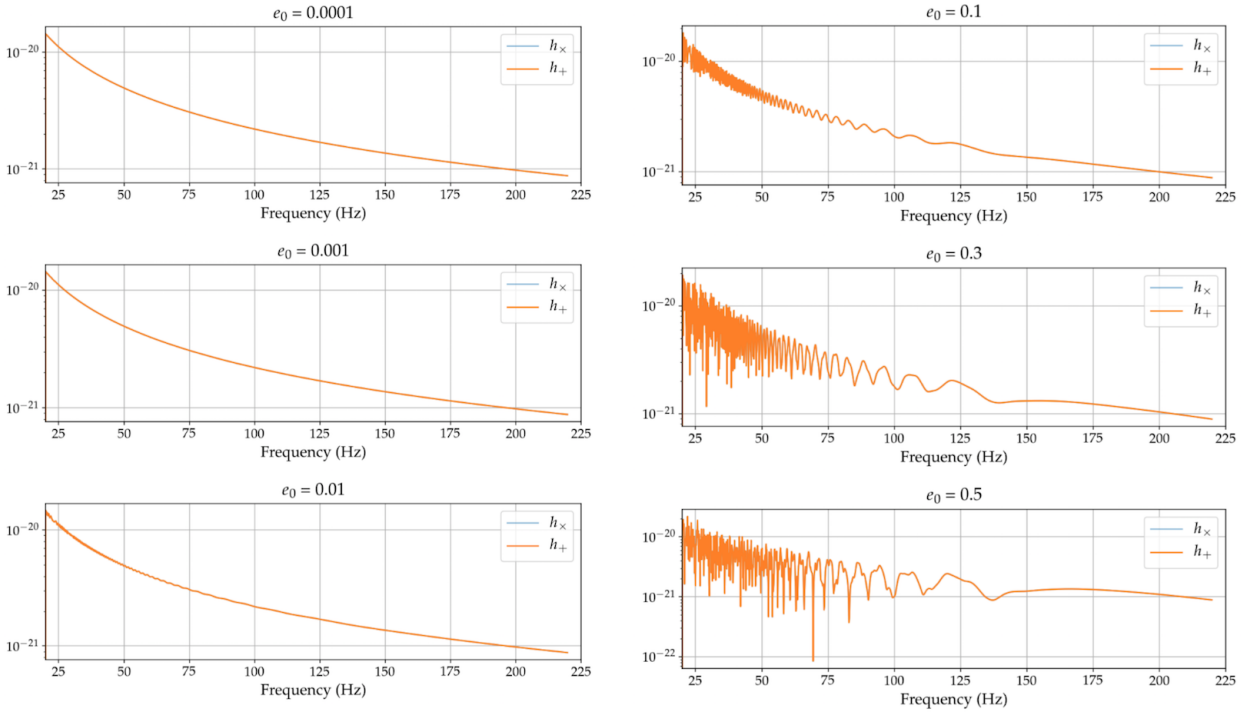

FIG. 10: Magnitude of frequency series waveforms generated with the EccentricFD approximant at initial eccentricities e_0=[0.0001, 0.001, 0.01, 0.1, 0.3, 0.5]. All waveforms are from a source with a distance of 1 megaparsec and masses $m_1 = m_2 = 10M_\odot$. The frequency axis shows the range 20 Hz to 225 Hz. Waveform model from [11].

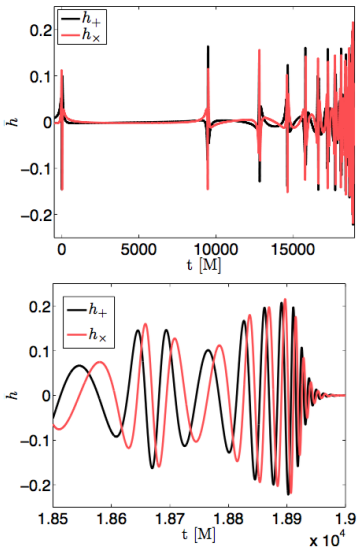

FIG. 11: Gravitational wave strain plot generated by the model described in East et al. for a periastron $r_p = 0.8M$ and an eccentricity e = 1. The top panel shows the entire waveform; the bottom panel shows a zoomed-in view of the end of the waveform. Figure from [10]

VI. BAYESIAN FRAMEWORK

Bayesian inference is the leading tool in parameter estimation in gravitational wave science. In the context of GW parameter estimation, data is compared with a parametrized model. Bayes' Theorem can be used to calculate a posterior probability density distribution for the model parameters as follows:

$$p(\vec{\theta}\,|\,d,H) = \frac{p(d\,|\,\vec{\theta},H)\,p(\vec{\theta}\,|\,H)}{p(d\,|\,H)} \tag{17}$$

where $\vec{\theta}$ is a vector containing unknown parameters, $d = \{d_1, d_2, \ldots, d_{\mathrm{N}_f}\}$ is the data represented as strain measurements in N_f discrete frequency bins, and H is a given model. $p(\vec{\theta}\,|\,d,H)$ is the *posterior*, or the probability that the gravitational wave strain was generated by a system with certain set of parameters $\vec{\theta}$ given the data d and assuming a particular model H. $p(d\,|\,\vec{\theta},H)$ is known as the *likelihood*, also represented with the letter $\mathcal{L}$. The likelihood is the probability of measuring the data d given a set of parameters and assuming a particular model. $p(\vec{\theta}\,|\,H)$ is the *prior*, representing prior understanding of the distribution of the parameters in nature. For example, a trivial prior is that an angle must lie between 0 and 2π; a non-trivial prior could be a non-informative or Jeffrey's prior on eccentricity, which is proportional to the square root of the determinant of the Fisher information matrix. Finally, $p(d\,|\,H)$ is the *evidence*, a normalization constant that does not effect a single posterior distribution, but can be used to compare different models using Bayesian Model Comparison [8].

The function to calculate the likelihood distribution for data d and parameters $\vec{\theta}$ is:

$$\mathcal{L} = p(d\,|\,\vec{\theta}) = \mathcal{N}\exp\left(-\frac{1}{2}\langle h(\vec{\theta}) - d\,|\,h(\vec{\theta}) - d\rangle\right) \tag{18}$$

where $h(\vec{\theta})$ is the gravitational wave strain generated by a system with parameters $\vec{\theta}$ and $\mathcal{N}$ is an arbitrary constant that gets canceled out by the evidence term in the posterior distribution. The noise weighted inner product $\langle\, a\,|\,b\,\rangle$ is equal to:

$$\langle\, a\,|\,b\,\rangle = 4\Re\int_0^\infty \frac{\tilde{a}(f)\,\tilde{b^*}(f)}{S_n(f)}df \tag{19}$$

where $S_n(f)$ is a power-spectral density (PSD) for the noise in the system.

VII. INTERIM RESULTS

This section presents the results that have thusfar emerged from this project. Section A presents a quantitative measure of difference between the waveform model I generated using Python in Section V and the EccentricTD model in LALSuite [11]. In Section B, I introduce a means of exploring the difference between two waveforms: their phase evolution. In Section C, I present the results from attempting to recover an eccentric waveform injection using a quasi-circular, non-spinning waveform. Section D discusses recovering an eccentric waveform injection with an *eccentric* waveform, exploring the question: Is eccentricity measurable if we use an eccentric waveform family and all other parameters are known? Finally, Section E discusses the onset of the final portion of the project: looking for degeneracies between eccentric and other effects, like spin.

A. Overlap Between My Waveform and EccentricTD

As explained in Section V, the waveform model in generated in Python (see Figure 8) captures the qualitative features of an eccentric binary inspiral, but is not quantitatively accurate due to several approximations made in the derivation. Such approximations include using Newtonian definitions for energy and angular momentum. The EccentricTD model in LALSuite [11] is a more quantitatively accurate waveform template (see Figure 9). However, it is important to note that EccentricTD and EccentricFD do not include spin effects and the EccentricFD waveform looks noisy at high eccentricities for unknown but probably unphysical reasons. To compare my model with EccentricTD, I calculated overlaps between them. The equation to calculate overlap between two vectors a and b is given in (20):

$$\mathcal{O} = \left[\frac{\langle\, a \,|\, b \,\rangle}{\langle\, a \,|\, a \,\rangle^{1/2} \langle\, b \,|\, b \,\rangle^{1/2}} \right]_{max.t,\varphi} \tag{20}$$

where $\langle\, a \,|\, b \,\rangle$ is the noise weighted inner product between a and b (19). In this case, the two vectors a and b are the time series for the strain for my waveform and an EccentricTD waveform with the exact same input parameters. Overlap is a value between 0 and 1, where 1 indicates that a and b are the same vector and 0 indicates that they are completely different vectors. Essentially, the overlap between waveforms is their dot product in the

parameter space. Figures 12 and 13 show, in the mass and eccentricity space, the results of calculating overlap between a waveform generated as described in Section V A and waveform generated using the EccentricTD approximant with the same input parameters. Figure 12 shows overlap over an eccentricity range of 0.05 to 0.45, while Figure 13 zooms in on the low-eccentricity range (0.005 to 0.1), as it is more probable in nature [13].

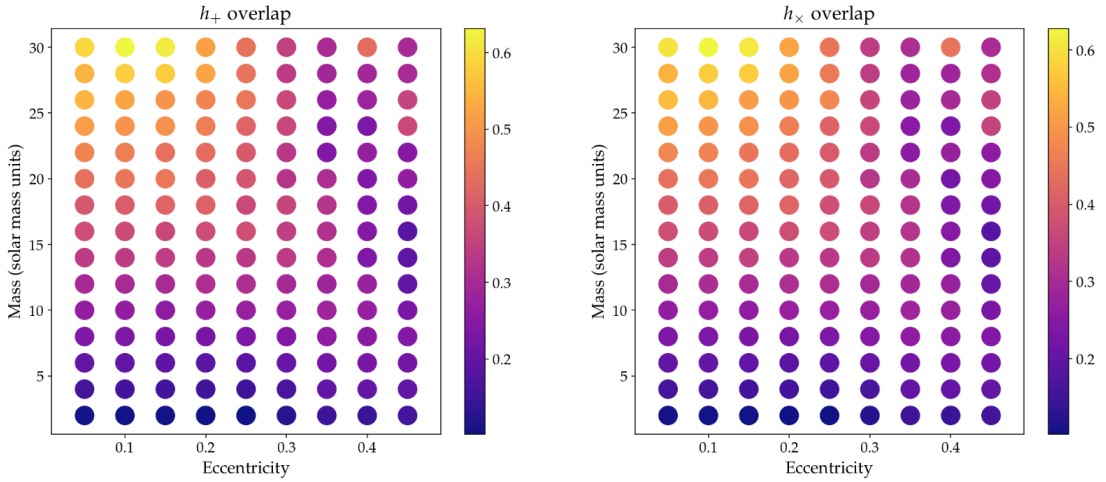

FIG. 12: Overlaps between a waveform generated as described in Section V A and waveform generated using the EccentricTD approximant with the same input parameters. Shown in the input parameter space of mass and eccentricity, with a mass range from 2 - 30 $M_\odot$ sampled every 2 $M_\odot$, and an eccentricity range of 0.05 - 0.45 sampled in increments of an eccentricity of 0.05. Overlaps calculating using *filter* package from [15].

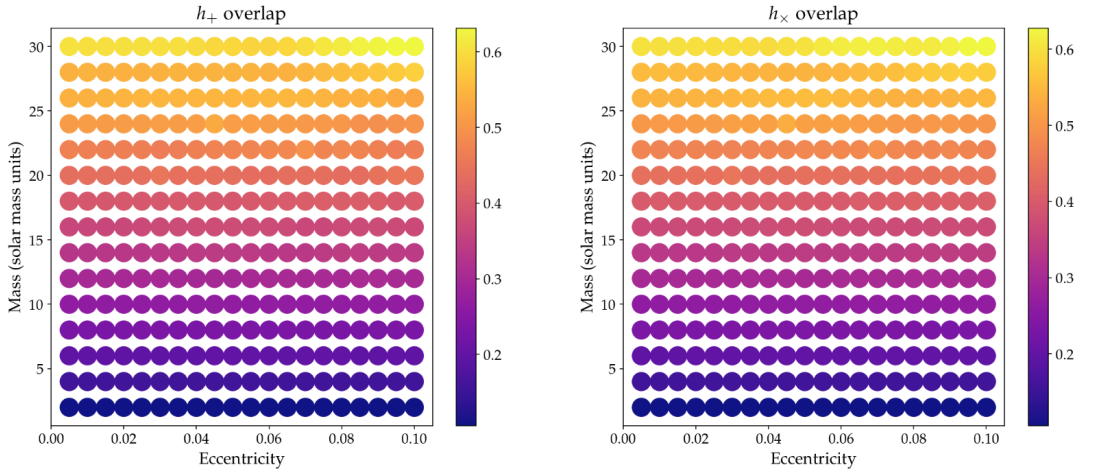

FIG. 13: Same as Fig. 12 but in different eccentricity range and higher sampling rate: a mass range from 2 - 30 $M_\odot$ sampled every 2 $M_\odot$, and an eccentricity range of 0.005 to 0.1, sampled in increments of an eccentricity of 0.005.

The dominant trends in these results are that: as mass increases, the overlap between the two waveforms increases; as eccentricity increases, the overlap decreases. As mass increases, the time the BBH spends in the LIGO band decreases, meaning the time series has less elements and thus less room for dissimilar elements between the two waveform models. As eccentricity increases, the bursts at periastron passage in the waveform become more pronounced, amplifying any differences between the two waveform models. The average overlap between the waveforms in the mass range 2 - 30 $M_\odot$ is listed in the following table:

e_0 **range**	**No. of data points**	**Average** h_+ **overlap**	**Average** $h_\times$ **overlap**
0.05 to 0.5	150	0.31504	0.31624
0.005 to 0.1	300	0.36644	0.36725

B. Differences in Phase Evolution for Eccentric vs. Non-Eccentric Waveforms

A potentially distinguishing feature of a waveform is its phase evolution. Phase can be extracted from the complex strain of a waveform: $h_c = h_+ + i\,h_\times$ where h_+ and $h_\times$ are the plus and cross polarizations of the gravitational wave. The phase evolution of waveforms with various eccentricities can be seen in Figure 14.

Subtracting the phase time series of an eccentric waveform from the phase time series of a waveform with negligible eccentricity yields the results seen in Figure 15. The larger the difference in eccentricity between two waveforms, the larger the difference in phase is between them. Additionally, as e_0 increases, the phase difference has a more pronounced sinusoidal component. Future work includes developing a quantitative function to describe this relationship.

Another characteristic of phase that draws interest is its derivative (see Figure 16). The relationship between phase of a gravitational wave and its frequency is:

$$\varphi(t) = \int_0^t 2\,\pi\, f_{GW}(t)\, dt \quad . \tag{21}$$

Therefore, the derivative of the phase is directly proportional to the frequency, $\dot{\varphi}(t) = 2\,\pi\, f_{GW}(t)$. In a non-eccentric case, the frequency of gravitational waves is calculated with equation (22), which is simplified to (23):

$$f_{GW}(t) = \frac{1}{\pi}\left(\frac{5}{256}\,\frac{1}{t_c\,-\,t}\right)^{3/8}\left(\frac{G\,M_c}{c^3}\right)^{-5/8} \quad , \tag{22}$$

$$f_{GW}(t) = 134\,Hz\left(\frac{1.21\,M_{sun}}{M_c}\right)^{5/8}\left(\frac{1}{t_c\,-\,t}\right)^{3/8} \quad . \tag{23}$$

Here, t_c is time of coalescence and M_c is chirp mass. Equations 21-23 are from [14]. Therefore, the derivative of the phase of a waveform with negligible eccentricity is equivalent:

$$\dot{\varphi}(t) = 2\,\pi\,134\,Hz\left(\frac{1.21\,M_{sun}}{M_c}\right)^{5/8}\left(\frac{1}{t_c\,-\,t}\right)^{3/8} \quad . \tag{24}$$

Future work for this project includes building upon this relationship to derive an equation relating $\dot{\varphi}(t)$ and eccentricity.

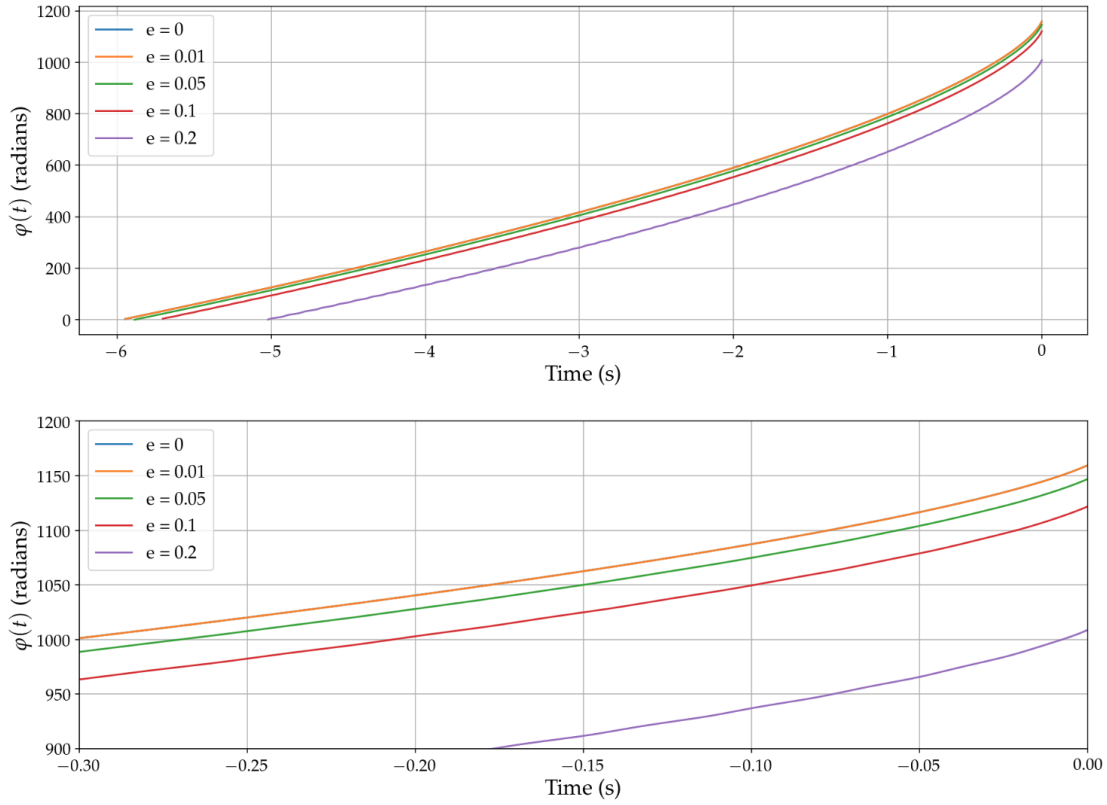

FIG. 14: The phase evolution of waveforms with various eccentricities. All have masses of $m_1 = m_2 = 10M_\odot$, a lower frequency of 20 Hz, and the rest of the parameters set to default. The top panel shows the phase evolution of the entire waveform; the bottom panel zooms in on the last 0.3 seconds before ISCO. In the legend, e refers to the eccentricity when the frequency of emitted GW is 20 Hz.

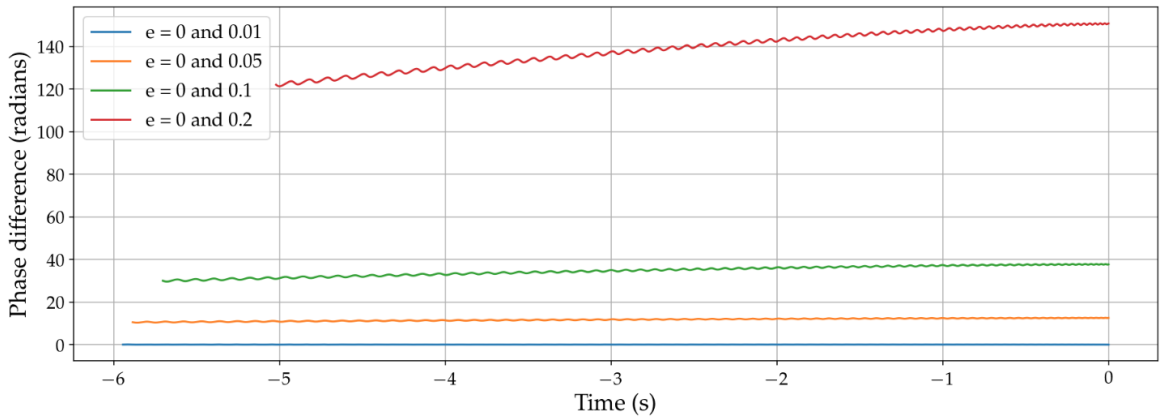

FIG. 15: Time series of the difference in phase between waveforms with and without eccentricity. All waveforms used have masses of $m_1 = m_2 = 10M_\odot$ and a lower frequency of 20 Hz. In the legend, e refers to the eccentricity when the frequency of emitted GW is 20 Hz.

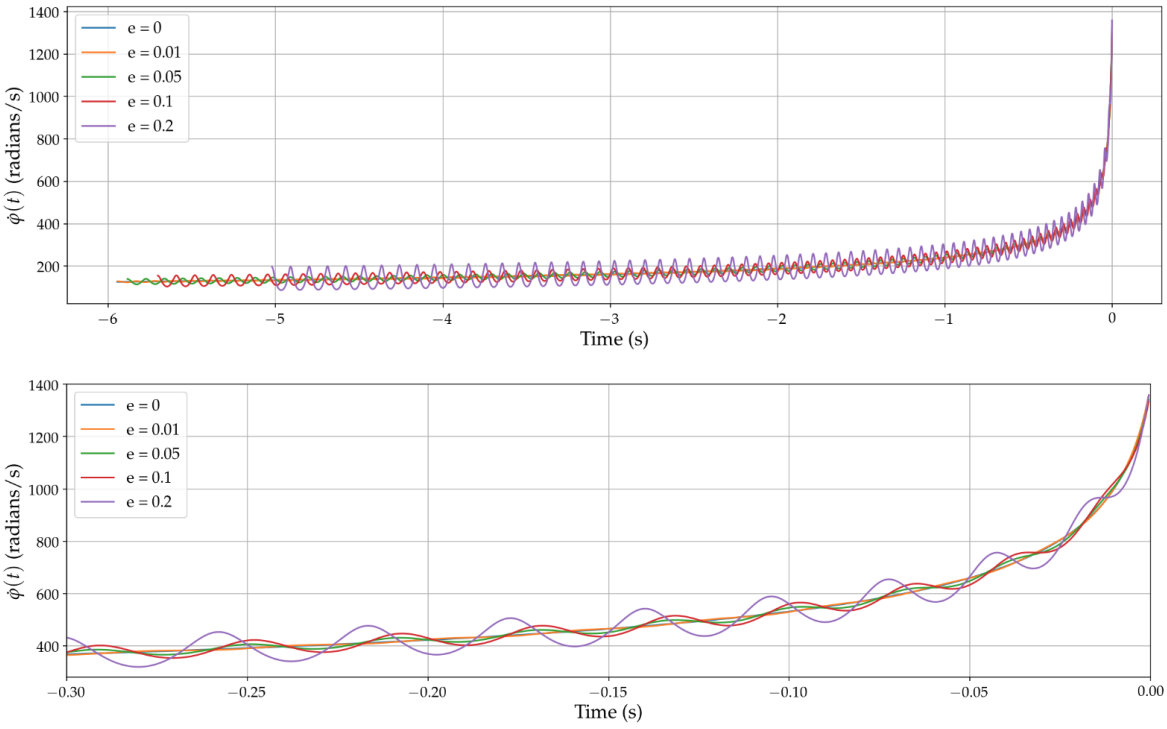

FIG. 16: The derivative of phase evolution for waveforms with various eccentricities. All have masses of $m_1 = m_2 = 10M_\odot$ and a lower frequency of 20 Hz. The top panel shows the derivative of phase evolution of the entire waveform; the bottom panel zooms in on the last 0.3 seconds before ISCO. In the legend, e refers to the eccentricity when the frequency of emitted GW is 20 Hz.

C. Recovering Eccentric Waveform with Quasi-Circular, Non-Spinning Template

If an incoming gravitational wave signal is from a source with an eccentric orbit and it is recovering using a template that assumes negligible eccentricity, the signal appears to have a lower SNR and our accuracy for estimating other parameters, e.g. mass, are compromised. The higher the eccentricity, the more SNR is lost when trying to recover this waveform using a quasi-circular template. This is shown in Figure 17. Currently, we are working on one-dimensional parameter estimation for mass using quasi-circular templates to recover eccentric injections. Results will be reported in the future.

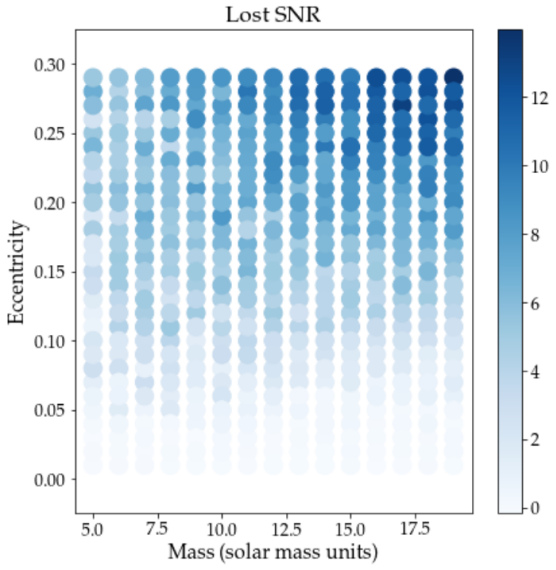

FIG. 17: SNR lost when using a template with no eccentricity to recover a waveform with eccentricity and the same mass parameters as the non-eccentric template. Shown in the input parameter space of mass and eccentricity of the injection, with a mass range from 5 - 20 $M_\odot$ sampled every 2.5 $M_\odot$, and an eccentricity range of 0.01 to 0.29, sampled in increments of an eccentricity of 0.05. All injections at a distance of 1000 MPc.

D. One Dimensional Parameter Estimation: Recovering Eccentric Waveform with Eccentric Template

In this section, we seek to discover how well the eccentricity parameter be extracted from an observed event when using a eccentric template to recover the waveform. We calculate a likelihood distribution using equation (18) in just the one-dimensional parameter

space of eccentricity, assuming all other parameters are known. Preliminary results for this calculation for an injected waveform with an eccentricity of $e_0 = 0.05$ are shown in Figure 18 for different systems with $m_1 = m_2 = [5, 20, 60]M_\odot$ and varying distances.

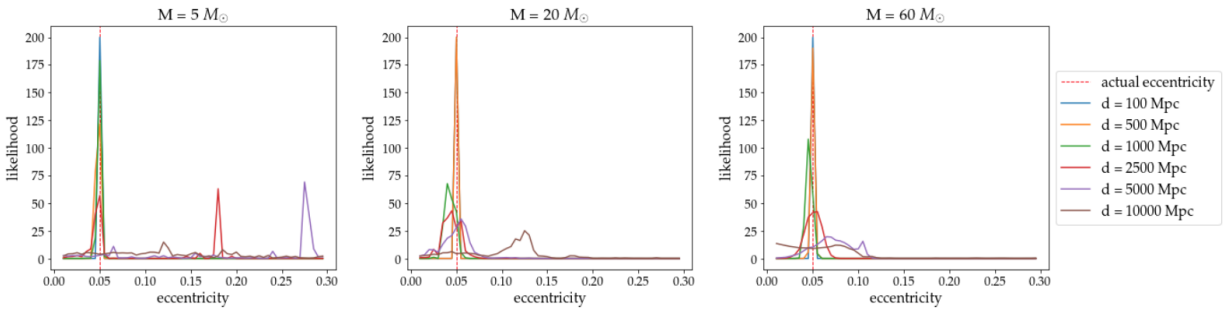

FIG. 18: One-dimensional likelihood distribution for recovering an EccentricTD injection ($e_0 = 0.05$) using an EccentricTD waveform with all parameter values the same except eccentricity. Data sampled at eccentricity increments of 0.005.

These preliminary results indicate that an eccentricity of 0.05 stops being able to be resolved when the system is at a distance between 1000 and 2500 Mpc for $m_1 = m_2 = 5M_\odot$ and between 500 and 1000 Mpc for $m_1 = m_2 = 20M_\odot$ or $60M_\odot$. In future work, these calculations will be repeated for more values of e_0 and more distances.

E. Two Dimensional Parameter Estimation: Recovering Eccentric Waveform with Non-Eccentric, Spinning Template

The remainder of this project focuses on searching for degeneracies between eccentricity and other effects. We look for degeneracies with both internal parameters, like spin and mass, and higher order effects such as spin precession. We plan to use LALinference to run Markov Chain Monte Carlos using Bayesian Inference to perform parameter estimation in a multi-dimensional parameter space. Until then, we just work in the two dimensional parameter space of spin and eccentricity. We inject an eccentric waveform and attempt to recover it using the SpinTaylorF2 approximant, a template without eccentricity but with non-zero aligned spin. We calculate the likelihood using (18) between the spinning waveform and the eccentric "data" at sample points in the parameter space of mass and spin.

Preliminary results of this process for an injected waveform with $e_0 = 0.1$ and a mass of 5 $M_\odot$ are shown in Figures 19 and 20. These results indicated that the best fit waveform

with spin for an eccentric injection has a non-zero spin and mass value slightly lower than the injected mass. We will repeat this process for different ejected eccentricity and mass combinations, and with different SNRs.

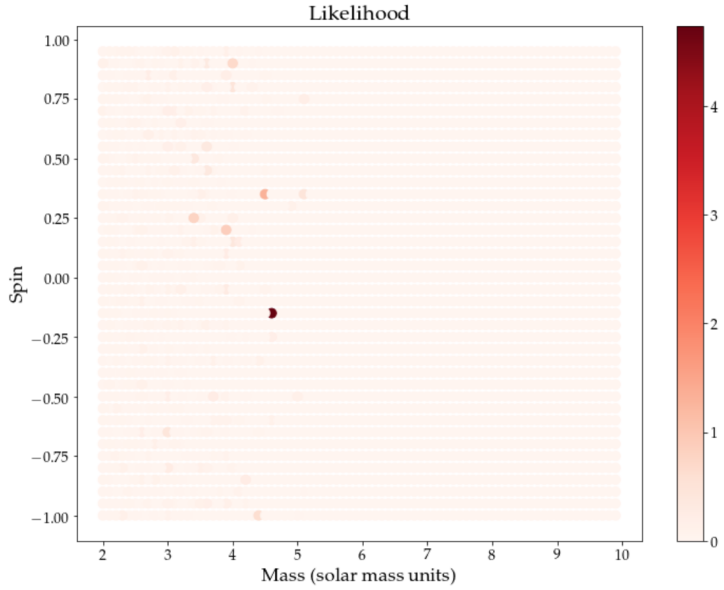

FIG. 19: 2-dimensional likelihood distribution in the mass-and-spin parameter space for fitting a SpinTaylorF2 aligned spin waveform to an injection generated with EccentricTD with $e_0 = 0.1$, a mass of $m_1 = m_2 = 5M_\odot$, and at a distance of 1000 Mpc. Distribution calculated for a mass range of 2 - 10 $M_\odot$ sampled every 0.1 $M_\odot$, and an spin range of -1.0 to 1.0, sampled in increments of spin of 0.05.

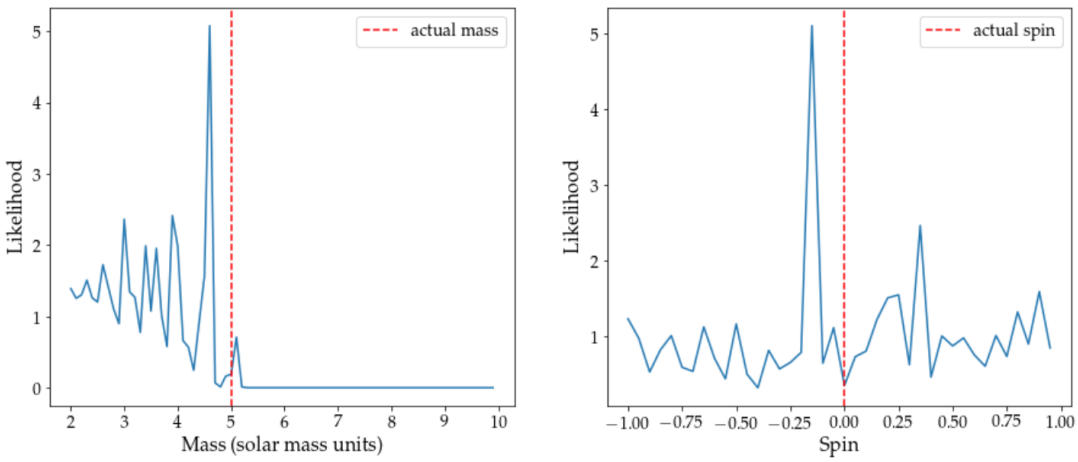

FIG. 20: The data displayed the plot in Fig. 19 projected onto the mass and spin axes.

Additionally, overlap was calculated using (20) at the same sample points in the mass-and-spin parameter space. The results are shown in Figure 21. All overlaps are less than 0.04,

meaning that even the best fit between the spinning and eccentric waveforms is very small. In other words, that the aligned-spin non-eccentric and non-spinning eccentric waveforms are very different, and should be very distinguishable from each other in data as long as the SNR is sufficiently high.

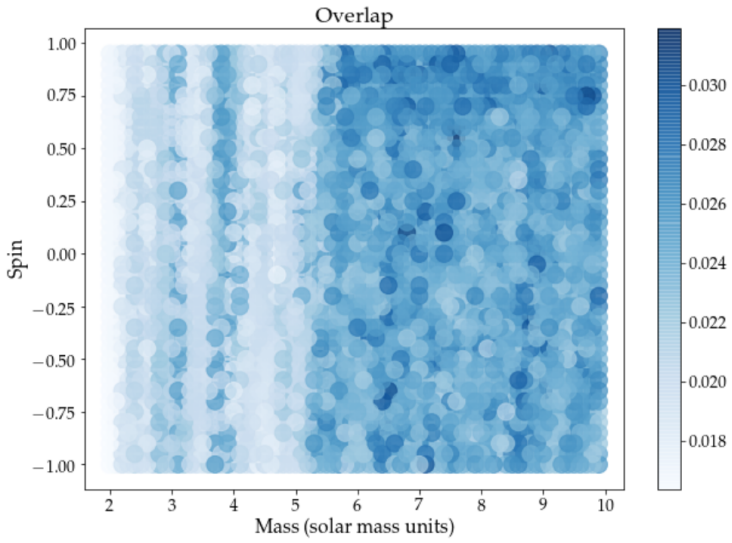

FIG. 21: Similar plot to Figure 19 but for overlap instead of likelihood.

VIII. CHALLENGES

The challenges I have faced this summer have primarily been in debugging Python code. To generate my eccentric waveform, I pulled equations from several different sources, each using different unit systems (SI, geometric, normalized by total mass, etc.) and ran into errors with correctly converting between different unit systems in Python. Additionally, often my code caused the Jupyter notebooks kernel to die when handling large quantities of data. I have had to work to make my code more optimized.

Another realm of challenges I have faced is juggling several different aspects of this project - waveform generation, characterizing phase evolution of a waveform, parameter estimation, looking for degeneracies - as well as different suggestions from mentors for what goals I should focus on. I have learned to balance and prioritize different goals based on my own interest as well as the interests of my mentors.

IX. FUTURE

My project schedule for the remainder of the summer is as follows:

Week 8: Continue one and two dimensional parameter estimation for recovering eccentric waveforms using eccentric templates to assess what values of eccentricity are detectable at what SNR. Repeat using aligned spin templates to recover eccentric waveforms. Begin LALinference runs to search for degeneracies between spin precession and eccentricity.

Week 9: Continue LALinference runs. Work on deriving functional fit for phase evolution as a function of eccentricity and time. Start final presentation.

Week 10: Work on final presentation and tie up loose ends.

---

[1] Abbott, B., et al. (LIGO Scientific Collaboration), "Astrophysical Implications of the Binary Black-Hole Merger GW150914," *Astrophys. J.*, LIGO-P1500262, (2016), [arXiv:1602.03846v1].

[2] Abbott, B., et al. (LIGO Scientific Collaboration and Virgo Collaboration), "Binary Black Hole Mergers in the First Advanced LIGO Observing Run," *Phys. Rev. X*, **6**, 041015, (2016).

[3] Abbott, B., et al. (LIGO Scientific Collaboration and Virgo Collaboration), "GW151226: Observation of Gravitational Waves from a 22-Solar-Mass Binary Black Hole Coalescence," Phys. *Rev. Lett.* **116**, 241103, (2016).

[4] Abbott, B., et al. (LIGO Scientific Collaboration and Virgo Collaboration), "GW170104: Observation of a 50-Solar-Mass Binary Black Hole Coalescence at Redshift 0.2" *Phys. Rev. Lett.* **118**, 221101 (2017).

[5] Abbott, B., et al. (LIGO Scientific Collaboration and Virgo Collaboration), "GW170608: Observation of a 19 Solar-mass Binary Black Hole Coalescence", *Astrophys. J.* **35**, 11pp (2017).

[6] Abbott, B., et al. (LIGO Scientific Collaboration and Virgo Collaboration), "GW170814: A Three-Detector Observation of Gravitational Waves from a Binary Black Hole Coalescence" *Phys. Rev. Lett.* **119**, 141101 (2017).

[7] Blanchet, Luc. "Gravitational Radiation from Post-Newtonian Sources and Inspiralling Com-

pact Binaries," *Living Rev. Relativity*, **17** /lrr-2014-2 (2014):http://www.livingreviews.org/lrr-20014-2.

[8] Biwer, C. M., et al. "PyCBC Inference: A Python-based parameterestimation toolkit for compact-object merger signals," (2018).

[9] Callister, Thomas A. "Improving Models of Eccentric Compact Binary Inspirals," University of Cambridge, (2014).

[10] East, William B., et al. "Observing complete gravitational wave signals from dynamical capture binaries", *Phys. Rev. D*, 87 (2013), [arXiv:1212.0837v2]

[11] LALSuite: Main Page, https://lscsoft.docs.ligo.org/lalsuite/

[12] LIGO Open Science Center, Data release for event GW150914, https://losc.ligo.org/events/GW150914/

[13] Lower, Marcus E., et al. "Measuring eccentricity in binary black hole inspirals with gravitational waves," (2018)

[14] Maggiore, Michele. *Gravitational Waves: Theory and Experiments*, Volume 1, Oxford University Press, (2008).

[15] PyCBC: Free and open software to study gravitational waves, https://pycbc.org/

[16] Randall, Lisa and Zhong-Zhi Xianyu. "Induced Ellipticity for Inspiraling Binary Systems," (2018), [arXiv:1708.08569v2]

[17] Randall, Lisa and Zhong-Zhi Xianyu. "Induced Ellipticity for Inspiraling Binary Systems,"An Analytical Portrait of Binary Mergers inHierarchical Triple Systems," (2018) [arXiv:1802.05718v1]

[18] Samsing, Johan. "Eccentric Black Hole Mergers Forming in Stellar Clusters," (2017), [arXiv:1711.07452]

[19] Sathyaprakasch, B.S and Bernard F. Schutz, Physics, Astrophysics, and Cosmology with Gravitational Waves, *Living Rev. Relativity*, lrr-2009-2, (2009): http://www.livingreviews.org/lrr-2009-2.

[20] Tiwari, V., et al. "A Proposed Search for the Detection of Gravitational Waves from Eccentric Binary Black Holes," *Phys. Rev. D*, 93 (2016), [arXiv:1511.09240]